Chapter 25

Reconstituting the Interaction Between Purified Nuclei and Microtubule Network

Gökçe Agsu, Jérémie Gaillard, Bruno Cadot, Laurent Blanchoin, Emmanuelle Fabre, and Manuel Théry

Abstract

The nucleus is the stiffest organelle in the cell. Several morphogenetic processes depend on its deformation such as cell migration, cell differentiation, or senescence. Recent studies have revealed various mechanisms involved in the regulation of nucleus stiffness and deformation. The implication of chromatin swelling, lamin density, actin filament, and microtubule network revealed that nucleus shape is the outcome of a fine balance between various sources of external forces and numerous means of internal resistance. In adherent cells, the actin network is the dominant player in external force production, whereas in nonadherent cells microtubules seem to take over. It is therefore important to set up reconstitution assays in order to decipher the exact contribution of each player in this mechanical balance. In this method, we describe a nucleus purification protocol that is suitable for nonadherent cells. We also show that purified nuclei can interact with microtubules and that nuclei purified from distinct cell types get differentially wrapped into the array of microtubules. A combination with a microtubule gliding assay offers the possibility to counterbalance the binding to the nucleus membrane by active motor-based forces pulling on microtubules. So this protocol allows an in-depth study of microtubule–nucleus interactions in vitro.

Key words Microtubule–nucleus interaction, Nucleus purification, Microtubule biochemistry, Reconstitution in vitro

1 Introduction

Nucleus has been suggested to be the stiffest organelle in the cell, and yet its shape can change during stem cell differentiation [1], cancer cell transformation [2], epithelial to mesenchymal transition [3], laminopathy-induced senescence [4, 5], nuclear import of YAP/TAZ [6], nuclear mechanosensing [7], release of neutrophil extracellular traps (also known as NETosis) [8], endothelial barrier crossing of leukocytes [9], and confined cell migration [10, 11]. In adherent cells, actin filaments regulate nuclear deformations. Dorsal actin cables apply forces on the nucleus with the

Hiroshi Inaba (ed.), *Microtubules: Methods and Protocols*,
Methods in Molecular Biology, vol. 2430, https://doi.org/10.1007/978-1-0716-1983-4_25,

involvement of focal adhesions and actomyosin network through the linker of nucleoskeleton and cytoskeleton (LINC) complex [12–16]. Microtubules (MTs) are also known to interact with nuclei during nuclear positioning and rotation [17–20] with the help of motors [21, 22] as well as DNA double-strand break (DSB) mobility and repair [23]. Additionally, in contrast to adherent cells, it seems to be MTs that regulate nuclear deformations in nonadherent cells. This has been documented in two independent studies on early [1] and terminal differentiation [24] of blood cells in humans. Former study shows that, during hematopoietic stem cell (HSC) differentiation into common myeloid progenitors (CMP), MT network reorganizes to form bundles along the nuclear membrane and deforms the nucleus by deep invaginations that result in chromatin remodeling and in alteration of the transcriptional program [1]. Similarly, human cytomegalovirus (CMV) infection is also able to orchestrate nucleus deformation using MT forces [25]. When infected a cell, CMV triggers *de novo* microtubule organizing center (MTOC) production, which polymerizes MTs binding to nuclear-bound dynein that results in the polarization of the nuclear envelope (NE) proteome. This viral-induced mechanical cascade causes nucleus deformation with consequences on chromatin architecture that eventually enhances the viral replication in the cell [25]. As exemplified above, there are many parameters that regulate the nucleus shape. Reconstitution assays in vitro appear complementary to cellular assays in order to investigate the specific role of defined parameters involved in nucleus deformation. Such reconstitution assays require a nucleus purification protocol that preserves the nuclear envelope intact. Previous nucleus purification protocols for adherent cells include cell scraping, a step that contributes to cell shearing and to purification yield, which cannot be applied to nonadherent cells [26, 27]. It is therefore necessary to develop a nucleus purification protocol to remove cell membrane without damaging the nuclear envelope in nonadherent cells. In the past, nuclei have been purified with detergents from nonadherent lymphocytes with the aim of studying the centrosome-nucleus association [28]. This detergent-based protocol results in high yield of purified nucleus. We aimed at developing a protocol without detergent in order to keep structure of the nuclear envelope as intact as possible. Here, we describe a nucleus purification protocol dedicated to nonadherent cells that allows to purify nuclei free of plasma membrane but with an intact nuclear envelope. We also describe a reconstitution assay in buffer conditions that are compatible with gliding assay where kinesin-1 motors and nucleus-bound dynein compete for MT interaction.

2 Materials

2.1 Flow Chamber Assembly

1. 1 M NaOH.
2. 96% EtOH.
3. Coverslip (thickness: 1, 20 × 20 mm, Knittel Glass).
4. Microscope slides (3 × 1 inch, Knittel Glass).
5. Coverslip mini-rack.
6. Slide mini-rack.
7. Double-tape spacer (thickness: 70 μm).
8. Metallic tweezers to handle glass coverslips.
9. Glass beaker for washing and stocking clean coverslips.
10. Sonicator.

2.2 Microtubule Polymerization and Taxol Stabilization

1. Tubulin: Systematically purified and labeled in our lab as described in Triclin et al. [29]. Briefly, tubulin was purified from fresh bovine brain by three cycles of temperature-dependent assembly and disassembly in Brinkley Buffer 80 (BRB80 buffer; BRB buffer: 80 mM PIPES, pH 6.8, 1 mM EGTA, and 1 mM $MgCl_2$ plus 1 mM GTP) [30]. MAP-free neurotubulin was purified by cation-exchange chromatography (EMD SO, 650 M, Merck) in 50 mM PIPES, pH 6.8, supplemented with 1 mM $MgCl_2$ and 1 mM EGTA [31]. Purified tubulin was obtained after a cycle of polymerization and depolymerization.
2. Fluorescent tubulin (ATTO-565-labeled tubulin) was prepared as previously described [32]. Microtubules from neurotubulin were polymerized at 37 °C for 30 min and layered onto cushions of 0.1 M NaHEPES, pH 8.6, 1 mM $MgCl_2$, 1 mM EGTA, 60% (v/v) glycerol, and sedimented by high centrifugation at 30 °C. Then microtubules were resuspended in 0.1 M NaHEPES, pH 8.6, 1 mM $MgCl_2$, 1 mM EGTA, 40% (v/v) glycerol, and labeled by adding 1/10 volume of 100 mM NHS-ATTO (ATTO Tec) for 10 min at 37 °C. The labeling reaction was stopped using 2 volumes of 2× BRB80, containing 100 mM potassium glutamate and 40% (v/v) glycerol, and then microtubules were sedimented onto cushions of BRB80 supplemented with 60% glycerol. Microtubules were resuspended in BRB80, and a second cycle of polymerization and depolymerization was performed before use (*see* **Note 1**).
3. BRB80: 80 mM PIPES, pH 6.8, 1 mM EGTA, 1 mM $MgCl_2$.
4. Taxol buffer: 10 μM Taxol in BRB80 0.5×.
5. Tubulin premix: BRB80 1× with 20 mM $MgCl_2$, 5 mM GTP, 1/4 volume of DMSO.

6. Milli-Q H_2O.
7. Thermo-mixer suitable for Eppendorf tubes.

2.3 Purification of Intact Nucleus from Nonadherent Cells

1. Hypotonic buffer: 9 mM HEPES pH 7.4, 0.9 mM KCl, 1.35 mM $MgCl_2$, 0.5 mM dithiothreitol (DTT), 1% protease inhibitor cocktail, 10% IMDM or RPMI medium for HSC or Jurkat, respectively.
2. Sucrose buffer: 20 mM HEPES pH 7.4, 25 mM KCl, 5 mM $MgCl_2$, 0.25 M sucrose, 100 mM ATP, 10 μg/mL Hoechst.
3. HSCs are isolated from human cord blood through CD34 selection as described in Biedzinski et al. 2020 [1]. Briefly, all human umbilical cord blood samples collected from normal full-term deliveries were obtained after mothers' written and informed consent, following the Helsinki's Declaration and Health Authorities. Cord blood samples came from the biological resource center, Saint-Louis Hospital Cord Blood Bank (Paris, France) authorized by French Cord Blood Network (AC 2016-2756, French Biomedical Agency, Paris, France). Mononuclear cells were collected using Ficoll separation medium (Eurobio, Courtaboeuf, France). CD34+ cells were further selected using Miltenyi magnetically activated cell sorting (MACS) columns (Miltenyi Biotech, Paris, France) according to the manufacturer's instructions. CD34+ cells were then either put in culture or frozen at −80 °C in IMDM (Gibco) supplemented with 10% fetal bovine serum (FBS) and 10% DMSO (WAK Chemie Medical GmbH). Freshly isolated CD34+ or thawed cells were allowed to recover overnight at 37 °C in IMDM supplemented with 10% FBS and antibiotics (Antibiotic-antimycotic, Sigma-Aldrich).
4. Sterile PBS.
5. Dounce homogenizer (size: 2 mL).

2.4 Reconstitution of Nucleus–Microtubule Interaction in Bulk

1. Polymerized and Taxol-stabilized MTs prepared in Subheading 3.2 (hereafter named MT stock).
2. Purified HSC or Jurkat nuclei prepared in Subheading 3.3 (hereafter named nuclei).
3. Saturation buffer at room temperature: 1% (w/v) BSA in HKEM (10 mM HEPES pH 7.2, 50 mM KCl, 1 mM EGTA, 5 mM $MgCl_2$).
4. Wash buffer at room temperature: 10 mM HEPES, 16 mM PIPES pH 6.8, 50 mM KCl, 5 mM $MgCl_2$, 1 mM EGTA, 20 mM DTT, 3 mg/mL glucose, 20 μg/mL catalase, 100 μg/mL glucose oxidase, 0.3% BSA supplemented with 10 μM Taxol.

5. ATP buffer on ice until usage: 10 mM HEPES, 16 mM PIPES pH 6.8, 50 mM KCl, 5 mM $MgCl_2$, 1 mM EGTA, 20 mM DTT, 3 mg/mL glucose, 20 μg/mL catalase, 100 μg/mL glucose oxidase, 0.3% BSA, 8 mM ATP, 0.2% methyl cellulose supplemented with 20 μM Taxol.
6. Freshly assembled flow chambers in Subheading 3.1.
7. Kimtech wipes (or Whatman paper).
8. Valap sealant (prewarmed mixture of equal weight of Vaseline, lanolin, and paraffin).

2.5 Reconstitution of Nucleus–Gliding Microtubule Interaction

1. MT stock and nuclei stock prepared in Subheadings 3.3 and 3.4.
2. Saturation buffer, wash buffer, and ATP buffer used in Subheading 2.4.
3. 200 nM GFP-tagged kinesin-1 in wash buffer on ice. Truncated kinesin-1 motor protein was purified using bacterial expression as previously described [34]. Plasmid for the kinesin construct, pET17_K560_GFP_His, was purchased from Addgene (15219, Cambridge, MA). Recombinant, truncated kinesin-1 motor protein fusion proteins were transfected into Rosetta2 (DE3)-pLysS E. coli (VWR), and expression was induced with 0.2 mM IPTG for 16 h at 20 °C. Harvested cells were resuspended in buffer A (50 mM sodium phosphate buffer pH 8, 250 mM NaCl) containing 0.1% Tween-20, 0.5 mM ATP, and 3 protease inhibitors (Roche) and lysed by sonication. The lysates were centrifuged 30 min at 25,000× *g* and 4 °C. We added 20 mM imidazole to the clear lysates, which were loaded onto an NiSepharose HP column (GE Healthcare). The column was washed with buffer B (50 mM sodium phosphate buffer pH 6, 250 mM NaCl, 1 mM $MgCl_2$, 0.1 mM ATP). Proteins were eluted in buffer C (50 mM sodium phosphate buffer pH 7.2, 250 mM NaCl, 500 mM imidazole, 1 mM $MgCl_2$, 0.1 mM ATP) then desalted into PEM-100 buffer containing 0.1 mM ATP, and snap-frozen in liquid nitrogen.
4. 0.2 mg/mL Anti-GFP antibody (Invitrogen) at kept on ice.

3 Methods

3.1 Flow Chamber Assembly

1. Place coverslips and microscope slides in their special mini-racks and place them in glass beakers. Fill the beakers with 1 M NaOH.
2. Cover the top of the beakers with parafilm and sonicate for 30 min.

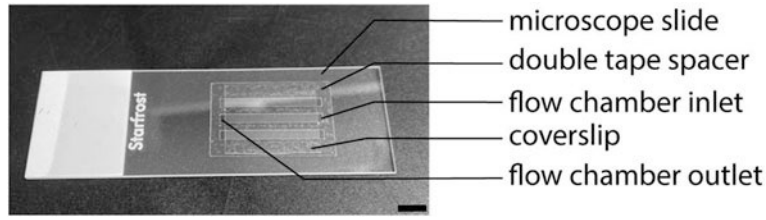

Fig. 1 Assembled flow chamber. Scale bar 500 mm

3. Discard NaOH solution and fill the beakers with Milli-Q three times.
4. Discard the Milli-Q and fill the beakers with 96% EtOH in order to wash for 30 min (*see* **Note 2**).
5. Wash the coverslips and slides one by one sequentially in three Milli-Q buckets with the help of tweezers.
6. Assemble the flow chamber with one dry coverslip and one dry slide using a double-sided tape spacer to create a channel (*see* **Notes 3** and **4**) (Fig. 1).

3.2 Microtubule Polymerization and Taxol Stabilization

In this subheading, we give instructions for MT polymerization in vitro and Taxol stabilization as previously described in Triclin et al. 2021 [29]. Briefly:

1. Prepare tubulin premix and keep it at room temperature.
2. Prepare Taxol buffer and keep it at room temperature.
3. Prepare 70 μM tubulin mix with 20% illumination (20% ATTO565-labeled tubulin and 80% nonlabeled tubulin) in BRB80 1×.
4. Set hot plate at 37 °C.
5. Initiate the microtubule polymerization by adding 1 volume of tubulin premix to 4 volumes of tubulin mix within an Eppendorf tube. Mix by gentle tapping.
6. Place the tube in thermo-mixer at 37 °C and incubate for 30 min (*see* **Note 5**).
7. Stabilize the MT polymerization by adding half volume of Taxol buffer and mix by gentle tapping (Fig. 2).
8. Protect from light with aluminum foil wrap and keep at room temperature (*see* **Notes 6** and **7**).

3.3 Purification of Intact Nucleus from Nonadherent Cells

In this section, we describe a hypotonic shock-based nuclei purification protocol that has been adapted for nonadherent HSCs and immortalized human T lymphocytes, Jurkat cells. This protocol allowed us to preserve the dynein population that is bound to the NE in both of the cell types.

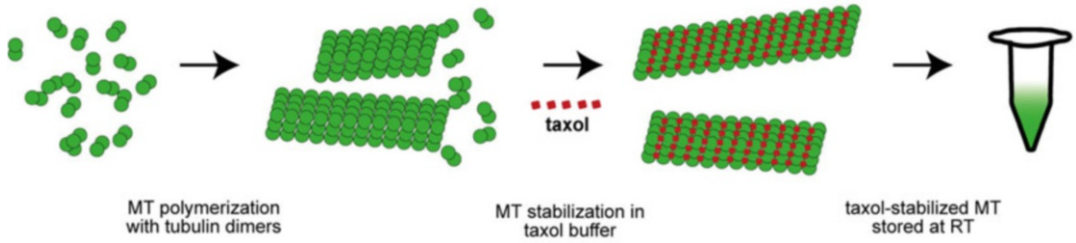

Fig. 2 MT polymerization and Taxol stabilization. MT polymerization is initiated with initially purified and fluorescent-labeled tubulin dimers in BRB80 buffer at 37 °C for 30 min. When MTs reach sufficient length (20–30 μm of length after around 30 min of polymerization in the abovementioned biochemical conditions), the polymerization process is stopped upon Taxol addition

1. Collect 1 mL (nearly 500 K cells) of CD34+ HSCs or Jurkats in a falcon tube that contains 4 mL of PBS.
2. Centrifuge at 244 × *g* for 5 min.
3. Remove the supernatant and resuspend pellet in 5 mL of PBS.
4. Centrifuge at 244 × *g* for 5 min.
5. Remove the supernatant by inverting the falcon tube upside down carefully and drying the tip with Kimtech wipe.
6. Add 500 μL of hypotonic buffer to the pellet, resuspend immediately, and transfer it in the homogenizer container incubated in ice (*see* **Note 8**).
7. Incubate on ice for 5 min.
8. Apply mechanical shearing with 30 up/down strokes using the glass grinder (Fig. 3).
9. Transfer the liquid in the homogenizer container into a pre-cooled 1.5 mL Eppendorf tube.
10. Centrifuge at 500 × *g* for 5 min at 4 °C (Fig. 3).
11. Eliminate the supernatant by inverting the Eppendorf tube on a Kimtech wipe and wash again with 500 μL of hypotonic buffer.
12. Gently vortex for 2 s.
13. Centrifuge at 500 × *g* for 5 min at 4 °C (Fig. 3).
14. Eliminate the supernatant and use again a Kimtech wipe in order to completely remove the remaining liquid in the Eppendorf tube.
15. Add 100 μL of sucrose buffer and gently resuspend the pellet (*see* **Notes 9** and **10**).

3.4 Reconstitution of Nucleus–Microtubule Interaction in Bulk

In this step, we describe how to assemble Taxol-stabilized MTs and purified nuclei together. This step requires proper biochemical conditions where nuclei do not shrink due to high salt

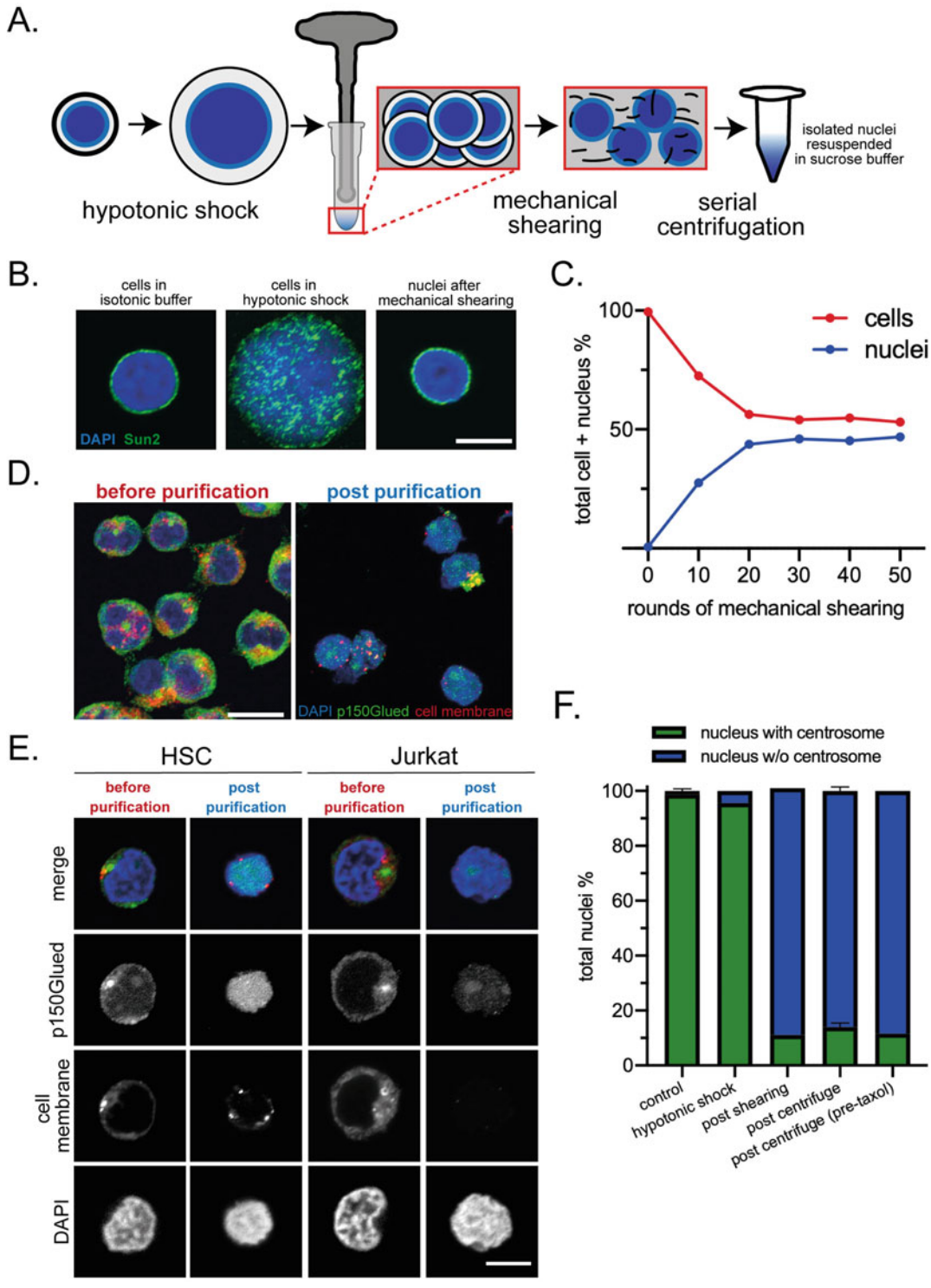

Fig. 3 Nucleus purification principles and results. (**a**) Illustration of purification method. Nonadherent HSCs or Jurkats are collected and resuspended in hypotonic buffer in order to render cell membrane more fragile to mechanical shearing. After 5 min of incubation on ice, cell membrane is mechanically sheared upon 30 up and down homogenizer strokes. Next, serial centrifugation is performed in order to remove the cytoplasm and cell

concentration of the MT buffer, and MTs remain stabilized in final Taxol concentration of 10 μM.

1. Add 5 μL of saturation buffer into the flow chamber and incubate for 3 min. Wash the flow chamber with 5 μL of wash buffer (*see* **Note 11**).
2. Mix 3 μL of MT stock with 47 μL of wash buffer. The aim is to dilute the amount of MTs added in the chamber to track individual MTs more easily (*see* **Notes 6** and **9**).
3. Mix 10 μL of diluted MTs, 10 μL of nuclei, and 10 μL of ATP buffer in a new Eppendorf tube.
4. Load 10 μL of the mix in the flow chamber (*see* **Note 12**).
5. Once sealed, put the flow chamber in the microscope's pre-heated incubator at 37 °C and initiate image acquisition. We acquired images of the full nucleus stack every 15 s for 30 min on Nikon spinning disk confocal microscope (Fig. 4).

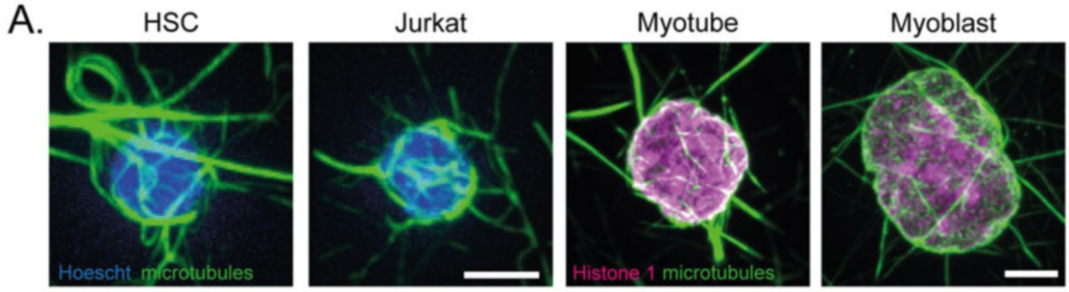

Fig. 4 MT network interacts with purified nuclei from various nonadherent and adherent cell lines. When co-loaded in the flow chamber, Taxol-stabilized MTs and purified nuclei were able to interact in 3D upon bundling and buckling along the nuclear membrane (HSC and Jurkat). In order to validate the reproducibility of our MT–nucleus interaction reconstitution method, we tested our protocol on nuclei purified from different cell types, including adherent mouse myoblast and myotube cells [33]. When we used the reconstitution protocol on purified myoblast and myotube nuclei with same amount of MTs, we could recapitulate similar interaction and buckling events all around the nuclei (myotube and myoblast). This suggests that MT–nucleus crosstalk reconstitution assay can also be applied on adherent cell nuclei (scale bar: 5 μm)

Fig. 3 (continued) membrane remnants. Small pellet of isolated nuclei is resuspended in sucrose buffer and kept on ice for up to 3 h. (**b**) Nuclear envelope in the course of purification. (**c**) Cell/nucleus ratio after given rounds of homogenizer strokes. Plateau suggests 30 is optimal. (**d**) General comparison of cell and nuclei before and after the purification, respectively. (**e**) Detailed representation of nucleus purification yield on HSC and Jurkat cells. (**f**) Amount of centrosome-bound nuclei in the course of purification. We observe a sharp decrease after homogenization, where only 15% of the nucleus still bear centrosome. Pretreating cells with Taxol does not ameliorate the percentage (15% for pre-Taxol samples). (**b** and **e**: scale bar, 5 μm) (**d**: scale bar, 10 μm) *HSC* hematopoietic stem cell

3.5 Reconstitution of Nucleus–Gliding Microtubule Interaction

We established reconstitution in vitro in the context of gliding assay where kinesin-1 is coated on the clean glass surface of the flow chamber. Kinesin-1 coating was important to ensure that buffer conditions were compatible for molecular motor functioning. It also set a competition between dynein-based forces produced on the nuclear membrane and kinesin-based forces produced on the glass coverslip.

1. Add 5 μL of Anti-GFP antibody into the flow chamber and incubate for 3 min. Wash the flow chamber with 5 μL of saturation buffer.
2. Add 5 μL of GFP-tagged kinesin-1 in the flow chamber and incubate for 3 min. Then, wash with 10 μL of wash buffer.
3. Mix 3 μL of MT stock with 47 μL of wash buffer. The aim is to dilute the amount of MTs added in the chamber to track individual MTs more easily.
4. Mix 10 μL of diluted MTs, 10 μL of nuclei, and 10 μL of ATP buffer in a new Eppendorf tube.
5. Load 10 μL of the mix in the flow chamber.
6. Seal the flow chamber with valap (or any other equivalent sealing material) and initiate immediate image acquisition (Fig. 5).

4 Notes

1. Avoid using tubulin stocks older than 4–6 months as they are less efficient in MT polymerization.
2. Coverslips and slides can be stored in EtOH in tightly sealed containers for up to 1 week.
3. Protein coating yield and quality will depend on the cleanliness of the coverslips. Therefore, assembly of the flow chamber should be performed on the day of experiment.
4. Protect the flow chamber from dust and store in a box before usage. Seal the box with parafilm.
5. Longer incubation time yields in longer MTs.
6. Avoid harsh pipetting and always cut pipette tips before pipetting in order to prevent MT breakage.
7. Every batch of newly polymerized Taxol-stabilized microtubules can be stored up to 3–4 days at room temperature. During storage, MT annealing will take place and this will result in longer MTs in time.
8. Purification protocol on nonadherent cells does not require initial cell scraping, thanks to which the protocol is less destructive. However, hypotonic shock requires optimization

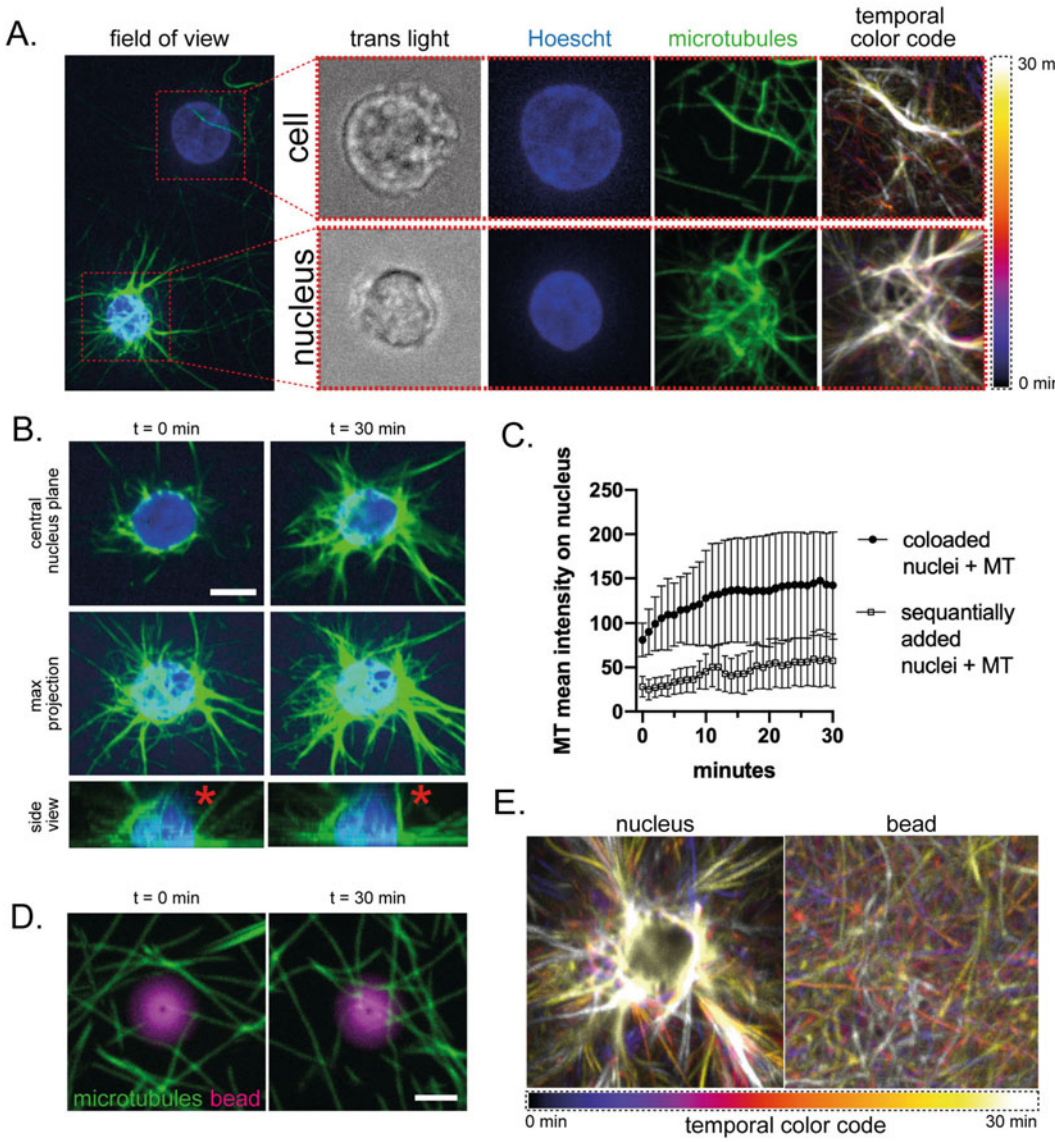

Fig. 5 In vitro reconstitution of MT networks with purified HSC nuclei. (**a**) Selective interaction of MTs with intact HSC and HSC nuclei. Live-imaging revealed that MTs did not specifically interact with intact cells and that MTs associated and interacted with purified nuclei (**b**). MT–nucleus interaction from various angles. Within 30 min of imaging, we observed a significant increase in the intensity of the MT network established around the nucleus. Once interacted with the purified nuclei, MTs remained buckled around it by making bundles along the nuclear membrane and by surrounding them upon 3D interaction (red asterisk). Side-view reconstructed images are interpolated. (**c**) Mean intensity of MT fluorescence on the nucleus surface in time. $N = 2$ (six nuclei for co-loaded condition, four nuclei for sequentially loaded condition). In the protocol Subheading 3.4, it is not recommended to do serial loading of purified elements in order to avoid nuclei being flushed out of the flow chamber. However, we tested the result of serial loading in our experimental work in order to illustrate the difference of MT–nucleus interaction between the options of co-loading and serial loading of purified elements. When added separately, MTs and nuclei have less interaction in time. (**d**) Carboxylated beads do not interact with motor-mobilized MTs. During live imaging, MTs remained completely mobile in the flow chamber and continued gliding on a kinesin-1-coated surface. (**e**) Motility of MTs in time with color code. Image taken every 15 s. Temporal analysis of MT gliding behavior revealed that HSC nuclei outcompeted kinesin-1 in MT interactions and strongly associated with MTs (Fig. 5e, left). Oppositely, MTs gliding near beads neither interacted with nor accumulated around them (Fig. 5e, right) (scale bar: 5 μm) (*see* **Notes 13** and **14**)

depending on the cell type. For instance, in an initial study, hypotonic-shock-based nucleus purification for HeLa cells required a stronger hypotonic shock [26], whereas in our protocol HSCs and Jurkats should be treated in milder hypotonic conditions.

9. ipette tip must be cut to prevent damage on the nucleus.
10. Purified nuclei can be stored in ice for up to 3 h. Do not freeze and thaw.
11. Asses the inlet and the outlet of the flow chamber before introducing the fluids (Fig. 1). Always introduce buffers using the same flow chamber inlet and apply flow in the same direction. Perform each wash step upon capillary action by introducing the wash buffer in the inlet and by placing a Kimtech wipe or Whatman paper in the outlet.
12. Avoid serial loading of purified elements. Co-incubate and co-load nuclei, MTs, and ATP buffer in order to make sure that nuclei are not washed off, that MTs are not broken due to multiple fluid flows, or that the ATP buffer is not diluted.
13. We describe a method to study MT–nucleus interaction in a reconstitution assay. For this purpose, we first established a nucleus purification protocol for nonadherent cell types. With cell membrane staining, we could show the plasma membrane was eliminated in HSCs and Jurkats. Our immunofluorescence results also show that the purification protocol yields purified nuclei with intact nuclear envelope as shown with Sun2 staining (Fig. 3b). Nuclei also retain dynein on the NE as shown with p150 Glued staining (Fig. 3e). We also showed that isolated nuclei can establish strong interaction with MTs which can resist the outward pulling forces applied by kinesin-1 (Fig. 5a). This protocol was also compatible with the purification and study of nuclei from various adherent cell types (Fig. 4). Overall, we were able to reconstitute in vitro the biochemical and mechanical balances of microtubule interactions with the outer surface of the nucleus.
14. It has been shown that nuclear-bound dynein transfers MT forces on the nucleus [35–37]. As dynein was present on purified HSC and Jurkat NE (Fig. 3e), we hypothesized that reconstitution of MT–nucleus interaction could lead to nucleus deformation upon MT-strangling. Indeed, nuclear-bound dynein has been shown to transfer MT forces on and deform the nucleus [1]. However, during live-imaging, we did not observe any nuclear deformations despite the presence of dynein and MTs. This result might imply that dynein motors are not functional despite their presence. Further work should be considered to better preserve the motor activity. The reconstitution buffer could not have been the limitation on dynein

activity, because the biochemical conditions were compatible for kinesin-1 functioning as confirmed with MT gliding (Fig. 5e). Therefore, the damage on dynein functionality likely happened in an earlier step during mechanical shearing (Fig. 3a). This is also the step where centrosome-bearing nuclei number sharply decreased by 85% (Fig. 3f). With further optimization, this assay would allow to reproduce nucleus deformation and study how it impacts lamin localization, chromatin remodeling, modulation of transcription, nuclear pore complex (NPC) positioning on NE, DSB repair, or any other specific process that could be downstream of MT–nucleus interactions.

Acknowledgments

This work was funded by grants from *Agence Nationale pour la Recherche* (ANR-14-CE11-0012, ANR-10-IHUB- 0002), from the European Research Council (ERC CoG 771599), from the Emergence program of the Ville de Paris, from the "Coups d'Elan" prize of the Bettencourt-Schueller foundation, and the Schlumberger foundation for education and research. GA received PhD fellowship from "Ecole Doctorale HOB N°561" and from "Fondation pour la Recherche Medicale" (grant FDT202001010927). The facility is supported by *Conseil Régional d'Ile-de-France, Cancerop*ôle *Ile-de-France, Université de Paris, Association Saint-Louis, Association Jean-Bernard, Fondation pour la Recherche Médicale*, French National Institute for Cancer Research (InCa) and *Ministère de la Recherche*.

References

1. Biedzinski S, Agsu G, Vianay B, Delord M, Blanchoin L, Larghero J, Faivre L, Théry M, Brunet S (2020) Microtubules control nuclear shape and gene expression during early stages of hematopoietic differentiation. EMBO J 39: e103957
2. Zink D, Fischer AH, Nickerson JA (2004) Nuclear structure in cancer cells. Nat Rev Cancer 4:677–687
3. Leggett SE, Sim JY, Rubins JE, Neronha ZJ, Williams EK, Wong IY (2016) Morphological single cell profiling of the epithelial–mesenchymal transition. Integr Biol 8:1133–1144
4. Sullivan T, Escalante-Alcalde D, Bhatt H, Anver M, Bhat N, Nagashima K, Stewart CL, Burke B (1999) Loss of A-type lamin expression compromises nuclear envelope integrity leading to muscular dystrophy. J Cell Biol 147:913–920
5. Scaffidi P, Misteli T (2006) Lamin A-dependent nuclear defects in human aging. Science 312:1059–1063
6. Cosgrove BD, Loebel C, Driscoll TP, Tsinman TK, Dai EN, Heo SJ, Dyment NA, Burdick JA, Mauck RL (2021) Nuclear envelope wrinkling predicts mesenchymal progenitor cell mechano-response in 2D and 3D microenvironments. Biomaterials 270:120662
7. Nava MM, Miroshnikova YA, Biggs LC, Whitefield DB, Metge F, Boucas J, Vihinen H, Jokitalo E, Li X, Hoffmann B, Merkel R, Niessen CM, Dahl KN, Arcos JMG, Wickström SA (2020) Heterochromatin-driven nuclear softening protects the genome against mechanical stress-induced damage. Cell 181:800–817
8. Brinkmann V, Reichard U, Goosmann C, Fauler B, Uhlemann Y, Weiss DS,

Weinrauch Y, Zychlinsky A (2004) Neutrophil extracellular traps kill bacteria. Science 303:1532–1535

9. Barzilai S, Yadav SK, Morrell S, Roncato F, Klein E, Stoler-Barak L, Golani O, Feigelson SW, Zemel A, Nourshargh S, Alon R (2017) Leukocytes breach endothelial barriers by insertion of nuclear lobes and disassembly of endothelial actin filaments. Cell Rep 18:685–699
10. Thiam HR, Vargas P, Carpi N, Crespo CL, Raab M, Terriac E, King MC, Jacobelli J, Alberts AS, Stradal T, Lennon-Dumenil A-M, Piel M (2016) Perinuclear Arp2/3-driven actin polymerization enables nuclear deformation to facilitate cell migration through complex environments. Nat Commun 7:10997
11. Venturini V, Pezzano F, Castro FC, Häkkinen HM, Jiménez-Delgado S, Colomer-Rosell M, Marro M, Tolosa-Ramon Q, Paz-López S, Valverde MA, Weghuber J, Loza-Alvarez P, Krieg M, Wieser S, Ruprecht V (2020) The nucleus measures shape changes for cellular proprioception to control dynamic cell behavior. Science 370:eaba2644
12. Makhija E, Jokhun DS, Shivashankar GV (2016) Nuclear deformability and telomere dynamics are regulated by cell geometric constraints. Proc Natl Acad Sci USA 113:E32–E40
13. Kim DH, Wirtz D (2015) Cytoskeletal tension induces the polarized architecture of the nucleus. Biomaterials 48:161–172
14. Buxboim A, Irianto J, Swift J, Athirasala A, Shin JW, Rehfeldt F, Discher DE (2017) Coordinated increase of nuclear tension and lamin-A with matrix stiffness outcompetes lamin-B receptor that favors soft tissue phenotypes. Mol Biol Cell 28:3333–3348
15. Almonacid M, Al Jord A, El-Hayek S, Othmani A, Coulpier F, Lemoine S, Miyamoto K, Grosse R, Klein C, Piolot T et al (2019) Active fluctuations of the nuclear envelope shape the transcriptional dynamics in oocytes. Dev Cell 51:145–157.e10
16. Davidson PM, Cadot B (2020) Actin on and around the nucleus. Trends Cell Biol. https://doi.org/10.1016/j.tcb.2020.11.009
17. Starr DA, Fridolfsson HN (2010) Interactions between nuclei and the cytoskeleton are mediated by SUN-KASH nuclear-envelope bridges. Annu Rev Cell Dev Biol 26:421–444
18. Reinsch S, Gönczy P (1998) Mechanisms of nuclear positioning. J Cell Sci 111:2283–2295
19. Cadot B, Gache V, Vasyutina E, Falcone S, Birchmeier C, Gomes ER (2012) Nuclear movement during myotube formation is microtubule and dynein dependent and is regulated by Cdc42, Par6 and Par3. EMBO Rep 13:741–749
20. Renkawitz J, Kopf A, Stopp J, de Vries I, Driscoll MK, Merrin J, Hauschild R, Welf ES, Danuser G, Fiolka R, Sixt M (2019) Nuclear positioning facilitates amoeboid migration along the path of least resistance. Nature 568:546–550
21. Metzger T, Gache V, Xu M, Cadot B, Folker ES, Richardson BE, Gomes ER, Baylies MK (2012) MAP and kinesin-dependent nuclear positioning is required for skeletal muscle function. Nature 484:120–124
22. Gache V, Gomes ER, Cadot B (2017) Microtubule motors involved in nuclear movement during skeletal muscle differentiation. Mol Biol Cell 28:865–874
23. Lottersberger F, Karssemeijer RA, Dimitrova N, de Lange T (2015) 53BP1 and the LINC complex promote microtubule-dependent DSB mobility and DNA repair. Cell 163:880–893
24. Olins AL, Olins DE (2004) Cytoskeletal influences on nuclear shape in granulocytic HL-60 cells. BMC Cell Biol 5:30
25. Procter DJ, Furey C, Garza-Gongora AG, Kosak ST, Walsh D (2020) Cytoplasmic control of intranuclear polarity by human cytomegalovirus. Nature 587:109–114
26. Guilluy C, Osborne LD, Van Landeghem L, Sharek L, Superfine R, Garcia-Mata R, Burridge K (2014) Isolated nuclei adapt to force and reveal a mechanotransduction pathway in the nucleus. Nat Cell Biol 16:376–381
27. Stephens AD, Liu PZ, Banigan EJ, Almassalha LM, Backman V, Adam SA, Goldman RD, Marko JF (2018) Chromatin histone modifications and rigidity affect nuclear morphology independent of lamins. Mol Biol Cell 29:220–233
28. Maro B, Bornens M (1980) The centriole-nucleus association: effects of cytochalasin B and nocodazole. Biol Cellulaire 39:287–290
29. Triclin S, Inoue D, Gaillard J, Htet ZM, DeSantis ME, Portran D, Derivery E, Aumeier C, Schaedel L, John K, Leterrier C, Reck-Peterson SL, Blanchoin L, Théry M (2021) Self-repair protects microtubules from destruction by molecular motors. Nat Mater. https://doi.org/10.1038/s41563-020-00905-0
30. Shelanski ML (1973) Chemistry of the filaments and tubules of brain. J Histochem Cytochem 21:529–539
31. Malekzadeh-Hemmat K, Gendry P, Launay JF (1993) Rat pancreas kinesin: identification and

potential binding to microtubules. Cell Mol Biol 39:279–285

32. Hyman A, Drechsel D, Kellogg D, Salser S, Sawin K, Steffen P, Wordeman L, Mitchison T (1991) [39] Preparation of modified tubulins. Methods Enzymol 196:478–485
33. Dean DA, Kasamatsu H (1994) Signal-and energy-dependent nuclear transport of SV40 Vp3 by isolated nuclei. Establishment of a filtration assay for nuclear protein import. J Biol Chem 269:4910–4916
34. Pierce DW, Vale RD (1998) [14] Assaying processive movement of kinesin by fluorescence microscopy. Methods Enzymol 298:154–171
35. Levy JR, Holzbaur EL (2008) Dynein drives nuclear rotation during forward progression of motile fibroblasts. J Cell Sci 121:3187–3195
36. Zhou K, Rolls MM, Hall DH, Malone CJ, Hanna-Rose W (2009) A ZYG-12–dynein interaction at the nuclear envelope defines cytoskeletal architecture in the C. elegans gonad. J Cell Biol 186:229–241
37. Fridolfsson HN, Ly N, Meyerzon M, Starr DA (2010) UNC-83 coordinates kinesin-1 and dynein activities at the nuclear envelope during nuclear migration. Dev Biol 338:237–250